Journal of Solid Mechanics Vol. 11, No. 1 (2019) pp. 26-38
DOI: 10.22034/JSM.2019.664214

Bending Behavior of Sandwich Plates with Aggregated CNT-Reinforced Face Sheets

M. Mirzaalian [1], F. Aghadavoudi [1,*], R. Moradi-Dastjerdi [2]

[1] *Department of Mechanical Engineering, Khomeinishahr Branch, Islamic Azad University, Khomeinishahr, Iran*
[2] *Young Researchers and Elite Club, Khomeinishahr Branch, Islamic Azad University, Khomeinishahr, Iran*

Received 4 September 2018; accepted 6 December 2018

ABSTRACT

The main aim of this paper is to investigate bending behavior in sandwich plates with functionally graded carbon nanotube reinforced composite (FG-CNTRC) face sheets with considering the effects of carbon nanotube (CNT) aggregation. The sandwich plates are assumed resting on Winkler-Pasternak elastic foundation and a mesh-free method based on first order shear deformation theory (FSDT) is developed to analyze the deflection of sandwich plates. In the face sheets, volume fraction of CNTs and their clusters are considered to be changed along the thickness. To estimate the material properties of the nanocomposite, Eshelby-Mori-Tanaka approach is applied. In the mesh-free analysis, moving least squares (MLS) shape functions are employed to approximate the displacement field and transformation method is used for imposition of essential boundary conditions. The effects of CNT volume fraction, distribution and degree of aggregation, and also boundary conditions and geometric dimensions are investigated on the bending behavior of the sandwich plates. It is observed that in the same value of cluster volume, FG distribution of clusters leads to less deflection in these structures.

Keywords: Bending; Aggregated carbon nanotube; Sandwich plates; Elastic foundation, Mesh-free method.

1 INTRODUCTION

THANKS to the remarkable and exceptional characteristics of carbon nanotubes, CNTs have stimulated a tremendous research on the prediction of their mechanical behavior since their discovery in 1990s [1]. Recently, CNTs have been wildly used in polymer based nanocomposite because of their high aspect ratio and low weight. The CNT/polymer structures which are supported by an elastic foundation are mainly used in concrete roads, raft, and mat foundations of buildings and reinforced concrete pavements of airport runways. To describe the interaction between the structure and foundation, Winkler and Winkler-Pasternak models are more used which are based on normal and normal-shear effects of the foundation, respectively [2]. Considering high cost of CNTs, optimization of the value of CNT volume fraction in nanocomposite is very important. On the other hand, mechanical properties of

*Corresponding author. Tel.: +98 31 33660011; Fax: +98 31 33660088.
E-mail address: davoodi@iaukhsh.ac.ir (F. Aghadavoudi).

CNTRC will become worse if the volume fraction of CNTs arises beyond certain limit [5]. Functionally graded materials (FGMs) are classified as a novel group of composite materials with gradient compositional variation. This concept could be incorporated to optimize the volume of consumed CNTs in the nanocomposites. The composites, which are reinforced by CNTs with grading distribution, are called functionally graded carbon nanotube reinforced composites and several works on these structures were carried out after FGM researches. In the first research about FG-CNTRC, Shen [3] presented nonlinear bending behavior of FG-CNTRC plates and showed that the linear FG distribution of CNTs can improve the reinforcement behavior. Based on three-dimensional theory of elasticity, Alibeigloo [4] discussed the static analysis of FG-CNTRC plate imbedded in piezoelectric layers with three cases of CNT distribution. Shariyat and Darabi [5] used a modified contact law to present the impact behavior of polymer/clay nanocomposite plates impacted by rigid spherical indenters. Pourasghar and Kamarian [6] presented natural frequencies of multi-walled carbon nanotubes (MWCNT) / polymer cylindrical panels based on three-dimensional theory of elasticity and modified Halpin-Tasi equations. Malekzadeh et al. [7] used FSDT and the differential quadrature method (DQM) to investigate on the free vibration behavior of quadrilateral laminated thin-to-moderately thick FG-CNTRC plates. Kundalwal and Meguid [8] investigated the effect of CNT waviness on the active constrained layer damping of the laminated hybrid composite shells by a three-dimensional finite element model. Mohammadimehr et al. [9] studied bending and biaxial buckling analyses of double-coupled FG boron nitride and carbon nanotubes reinforced plates using the modified strain gradient Reddy rectangular plate theory. Ghorbanpour Arani et al. [10]–[12] investigated the vibrational behavior of some miro/nano composite or CNT-reinforced nanocomposite structures using different theories.

Due to large aspect ratio (usually >1000) and low bending rigidity of CNTs, increasing of nanotube volume fraction could lead to CNT aggregation in the host matrix which dramatically decreased the overall effectiveness of CNT reinforcement. Pourasghar et al. [13] used Eshelby–Mori–Tanaka approach to estimate material properties of nanocomposite by considering the effects of CNT orientation and aggregation and studied free vibration analysis of FG-CNTRC cylinders based on both three-dimensional theory of elasticity. Sobhani Aragh and Hedayati [14] used the 2D GDQM to discretize the governing equations and to implement the boundary conditions and presented vibrational behavior of FG-CNTRC cylindrical panels based on the Eshelby– Mori–Tanaka approach. Tahouneh and Yas [15] used equivalent continuum model and Eshelby-Mori-Tanaka approach to study the vibrational behavior of thick annular FG-CNTRC plates resting on an elastic foundation. Also, refined, higher order and three-dimensional elasticity theories have been used for free vibration and biaxial buckling analyses of sandwich plates with nanocomposite face sheets reinforced by aggregated CNTs [16]–[18]. Moradi-Dastjerdi and Malek-Mohammadi [19] presented free vibration and buckling analyses of FG nanocomposite plates reinforced by aggregated nanotube by Eshelby–Mori–Tanaka approach and a four independent unknowns refined theory.

Mesh-free methods also have been used for analysis of FG-CNTRC structures. Lei et al. [20] used the element-free *kp*-Ritz method based on FSDT for analysis of buckling behavior in FG-CNTRC plates. Static, dynamic and transient heat transfer analyses of FG-CNTRC cylinders are examined by a weak form mesh-free method based on MLS shape functions [21]–[24]. Shams et al. [25] used reproducing kernel particle method (RKPM) based on modified FSDT and examined the effects of CNT aspect ratio and waviness on the buckling behavior of FG-CNTRC plates subjected to in-plane loads. Moradi-Dastjerdi et al. [26], [27] investigated the effects of CNTs orientation and aggregation on the stress distribution and wave propagation of axisymmetric FG-nanocomposite cylinders using a mesh-free method based on Eshelby–Mori–Tanaka approach. Zhang et al. [28], [29] used an element-free based improved moving least squares-Ritz (IMLS-Ritz) method and FSDT to study the buckling behavior FG-CNTRC plates resting on Winkler foundations and nonlinear bending of these plates resting on Pastenak elastic foundation. Finally, Moradi-Dastjerdi et al. [30], [31] used a mesh-free method based on first-order theory to analyze the static, free vibrational and dynamic responses of FG nanocomposite plates, reinforced by wavy single-walled carbon nanotubes which are resting on a Winkler-Pasternak elastic foundation.

In this paper as a new work, bending behavior of sandwich plates with FG-CNTRC face sheets which are resting on Winkler-Pasternak elastic foundation are investigated by a mesh-free method based on FSDT. In the face sheets, CNT volume fraction and their clusters are varied along the thickness. The effect of CNT aggregation in the face sheets is considered and the material properties of the nanocomposite are estimated based on Eshelby–Mori–Tanaka approach. The mesh-free method is based on MLS shape functions to approximate displacement field and transformation method to impose essential boundary conditions. The mentioned mesh-free method doesn't increase the calculations against Element-Free Galerkin (EFG). The effects of various parameters are investigated on the bending behavior of the sandwich plates.

2 MATERIAL PROPERTIES IN FG-CNTRC FACE SHEETS

In this paper, sandwich plates with an isotropic core and two symmetric FG-CNTRC face sheets resting on the Winkler-Pasternak elastic foundation are considered with length a, width b, each face sheet thickness h_f and total thickness h as shown in Fig. 1. The CNTRC face sheets are made from a mixture of aggregated single-walled carbon nanotubes (SWCNTs) and an isotropic matrix. The SWCNT reinforcement is either uniformly distributed (UD) or functionally graded along the face sheet thickness. So, the volume fraction of nanotubes, f_r, or volume of CNTs clusters are varied along the thickness as Fig. 2 and according to:

$$\begin{aligned} f_r &= \left[(2z-h)/(2h_f)+1\right]^n f_{r_{\max}} && \text{For top face sheet} \\ f_r &= 0 && \text{For core} \\ f_r &= \left[1-(2z-h)/(2h_f)\right]^n f_{r_{\max}} && \text{For bottom face sheet} \end{aligned} \tag{1}$$

where n and $f_{r_{\max}}$ are volume fraction power and maximum value of CNT volume fraction (which is occurred on the external faces), respectively. Many published studies had a different focus on mechanical properties of polymer nanotube composites. However, the common theme seems to have been enhancement of Young's modulus. In this section, the effective mechanical properties of this composite are obtained based on the Eshelby–Mori–Tanaka approach. Based on the Mori–Tanaka method, the complete elastic stiffness tensor for the composite is given as [32]:

$$C = C_m + f_r \left\langle (C_r - C_m) A_r \right\rangle \left(f_m I + f_r \left\langle A_r \right\rangle \right)^{-1} \tag{2}$$

where f_r and f_m are the fiber and matrix volume fractions, respectively, C_m is the stiffness tensor of the matrix material, C_r is the stiffness tensor of the fiber, I is the forth order identity tensor and A_r is the dilute strain-concentration tensor of the *r th* phase for the fiber which is given as:

$$A_r = \left[I + S (C_m)^{-1} (C_r - C_m) \right]^{-1} \tag{3}$$

The tensor S is Eshelby's tensor, as given by Eshelby [33] and Mura [34].

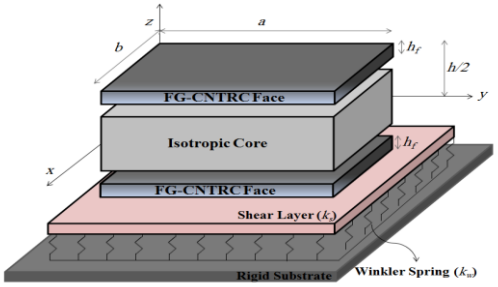

Fig.1
Schematic of the sandwich plate resting on Winkler-Pasternak elastic foundation.

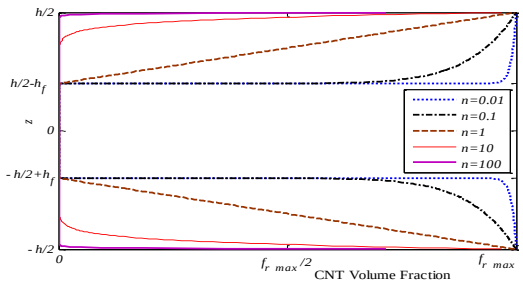

Fig.2
Variation of nanotube volume fraction (f_r) along the thickness of sandwich plate for different value of CNT volume fraction exponent.

But due to large aspect ratio, low bending rigidity and high value of volume fraction of CNTs and also Van der Waals forces, CNTs have a tendency to bundle or cluster together which is make them quite difficult to produce fully-dispersed CNT reinforced composites. The effect of nanotube aggregation on the elastic properties of randomly oriented CNTRC is presented in this section. Shi et al. [32] derived a two parameter micromechanics model to determine the effect of nanotube agglomeration on the elastic properties of randomly oriented CNTRC (Fig. 3). It is assumed that a number of CNTs are uniformly distributed throughout the matrix and the remained CNTs are aggregated in some cluster form, as shown in Fig. 3. The total volume of the CNTs in the representative volume element (RVE), denoted by V_r, can be divided into the following two parts:

$$V_r = V_r^{cluster} + V_r^{m} \tag{4}$$

where $V_r^{cluster}$ denotes the volume of CNTs inside a cluster, and V_r^{m} is the volume of CNTs in the matrix and outside the clusters. The two parameters used to describe the aggregation are defined as:

$$\mu = V_{cluster} / V \ , \ \eta = V_r^{cluster} / V_r \qquad 0 \le \mu, \eta \le 1 \tag{5}$$

where V is volume of RVE, $V_{cluster}$ is volume of clusters in the RVE. μ is the volume fraction of clusters with respect to the total volume V of the RVE, η is the volume ratio of the CNTs inside the clusters over the total CNT inside the RVE. When $\mu = 1$, this means uniform distribution of nanotubes throughout the entire composite without aggregation, and with the decreasing in μ, the agglomeration degree of CNTs is more severe. When $\eta = 1$, all the nanotubes are assumed located in the clusters. The case $\eta = \mu$ means that the volume fraction of CNTs inside the clusters is as same as that of CNTs outside the clusters (fully-dispersed).

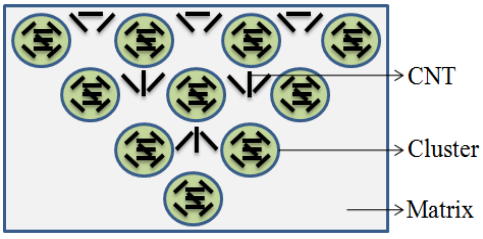

Fig.3
RVE with Eshelby cluster model of FG aggregation of CNTs.

Thus, we consider the CNT-reinforced composite as a system consisting of clusters of sphere shape embedded in a matrix. We may first estimate respectively the effective elastic stiffness of the clusters and the matrix, and then calculate the overall property of the whole composite system. The effective bulk modulus, K_{in}, and shear modulus, G_{in}, of the cluster can be calculated by Prylutskyy et al. [35], respectively:

$$K_{in} = K_m + \frac{f_r \eta (\delta_r - 3K_m \alpha_r)}{3(\mu - f_r \eta + f_r \eta \alpha_r)}, \quad G_{in} = G_m + \frac{f_r \eta (\eta_r - 3G_m \beta_r)}{2(\mu - f_r \eta + f_r \eta \beta_r)} \tag{6}$$

where

$$\alpha_r = \frac{3(K_m + G_m) + k_r - l_r}{3(G_m + k_r)} \tag{7}$$

$$\beta_r = \frac{1}{5}\left\{ \frac{4G_m + 2k_r + l_r}{3(G_m + k_r)} + \frac{4G_m}{G_m + p_r} + \frac{2\left[G_m(3K_m + G_m) + G_m(3K_m + 7G_m)\right]}{G_m(3K_m + G_m) + m_r(3K_m + 7G_m)} \right\} \tag{8}$$

$$\delta_r = \frac{1}{3}\left\{ n_r + 2l_r + \frac{(2k_r + l_r) + (3K_m + 2G_m - l_r)}{G_m + k_r} \right\} \tag{9}$$

$$\eta_r = \frac{1}{5}\left[\frac{2}{3}(n_r - l_r) + \frac{8G_m p_r}{G_m + p_r} + \frac{8m_r G_m (3K_m + 4G_m)}{3K_m (m_r + G_m) + G_m (7m_r + G_m)} + \frac{2(k_r - l_r)(2G_m + l_r)}{3(G_m + k_r)}\right] \tag{10}$$

k_r, l_r, m_r, n_r, and p_r are the Hill's elastic moduli for the reinforcing phase (transversely isotropic CNTs) which are reported in [32]. Also, the effective bulk modulus K_{out} and shear modulus G_{out} of the matrix outside the cluster can be calculated by [32]:

$$K_{out} = K_m + \frac{f_r(1-\eta)(\delta_r - 3K_m\alpha_r)}{3\left[1-\mu-f_r(1-\eta)+f_r(1-\eta)\alpha_r\right]} \tag{11}$$

$$G_{out} = G_m + \frac{f_r(1-\eta)(\eta_r - 2G_m\beta_r)}{2\left[1-\mu-f_r(1-\eta)+f_r(1-\eta)\beta_r\right]} \tag{12}$$

f_r and f_m are the volume fractions for carbon nanotube and matrix. Finally, the effective bulk modulus K and the effective shear modulus G of the composite are derived from the Mori-Tanaka method as follows [32]:

$$K = K_{out}\left[1 + \frac{\mu\left(\frac{K_{in}}{K_{out}} - 1\right)}{1 + \alpha(1-\mu)\left(\frac{K_{in}}{K_{out}} - 1\right)}\right], G = G_{out}\left[1 + \frac{\mu\left(\frac{G_{in}}{KG_{out}} - 1\right)}{1 + \beta(1-\mu)\left(\frac{G_{in}}{G_{out}} - 1\right)}\right] \tag{13}$$

with

$$\upsilon_{out} = \frac{3K_{out} - 2G_{out}}{2(3K_{out} + G_{out})}, \alpha = \frac{1+\upsilon_{out}}{3(1-\upsilon_{out})}, \beta = \frac{2(4-5\upsilon_{out})}{15(1-\upsilon_{out})} \tag{14}$$

The effective Young's modulus E and Poisson's ratio υ of the composite in the terms of K and G are given by:

$$E = \frac{9KG}{3K+G}, \upsilon = \frac{3K-2G}{6K+2G} \tag{15}$$

3 GOVERNING EQUATIONS

Based on the FSDT, the displacement components can be defined as [36]:

$$\begin{aligned} u(x,y,z) &= u_0(x,y) + z\,\theta_x(x,y) \\ v(x,y,z) &= v_0(x,y) + z\,\theta_y(x,y) \\ w(x,y,z) &= w_0(x,y) \end{aligned} \tag{16}$$

where u, v and w are displacements in the x, y, z directions, respectively. u_0, v_0 and w_0 denote midplane displacements, θ_x and θ_y rotations of normal to the midplane about y-axis and x-axis, respectively. The kinematic relations can be obtained as follows:

$$\begin{Bmatrix} \varepsilon_{xx} \\ \varepsilon_{yy} \\ \gamma_{xy} \end{Bmatrix} = \boldsymbol{\varepsilon_0} + z\boldsymbol{\kappa}\ ,\ \begin{Bmatrix} \gamma_{yz} \\ \gamma_{xz} \end{Bmatrix} = \boldsymbol{\gamma}_0 \tag{17}$$

where

$$\boldsymbol{\varepsilon}_0=\begin{Bmatrix}\partial u_0/\partial x\\ \partial v_0/\partial y\\ \partial u_0/\partial y+\partial v_0/\partial x\end{Bmatrix},\boldsymbol{\kappa}=\begin{Bmatrix}\partial\theta_x/\partial x\\ \partial\theta_y/\partial y\\ \partial\theta_x/\partial y+\partial\theta_y/\partial x\end{Bmatrix},\boldsymbol{\gamma}_0=\begin{Bmatrix}\partial v/\partial z+\partial w/\partial y\\ \partial u/\partial z+\partial w/\partial x\end{Bmatrix}=\begin{Bmatrix}\theta_y+\partial w_0/\partial y\\ \theta_x+\partial w_0/\partial x\end{Bmatrix} \tag{18}$$

The linear constitutive relations of a FG plate can be written as:

$$\begin{Bmatrix}\sigma_x\\ \sigma_y\\ \sigma_{xy}\end{Bmatrix}=\begin{bmatrix}Q_{11}(z) & Q_{12}(z) & 0\\ Q_{12}(z) & Q_{22}(z) & 0\\ 0 & 0 & Q_{66}(z)\end{bmatrix}\begin{Bmatrix}\varepsilon_x\\ \varepsilon_y\\ \gamma_{xy}\end{Bmatrix} or\ \boldsymbol{\sigma}=\mathbf{Q_b}(z)\boldsymbol{\varepsilon}\ ,\ \begin{Bmatrix}\sigma_{yz}\\ \sigma_{xz}\end{Bmatrix}=\alpha(z)\begin{bmatrix}Q_{44}(z) & 0\\ 0 & Q_{55}(z)\end{bmatrix}\begin{Bmatrix}\gamma_{yz}\\ \gamma_{xz}\end{Bmatrix} or\ \boldsymbol{\tau}=\alpha(z)\mathbf{Q}_z(z)\boldsymbol{\gamma} \tag{19}$$

In which α denotes the transverse shear correction coefficient, which is suggested as $\alpha=5/6$ for homogeneous materials. For FGMs, the shear correction coefficient is taken to be $\alpha=5/(6-(\upsilon_{CN}V_{CN}+\upsilon_m V_m))$ [37].

$$\begin{aligned}&Q_{11}(z)=\frac{1-\nu_{23}\,\nu_{32}}{E_2E_3\Delta}\ ,\ Q_{22}(z)=\frac{1-\nu_{31}\nu_{13}}{E_1E_3\Delta}\ ,\ Q_{12}(z)=\frac{\nu_{21}+\nu_{31}\nu_{23}}{E_2E_3\Delta}\\ &Q_{44}(z)=G_{23}\ ,\ Q_{55}(z)=G_{31}\ ,\ Q_{66}(z)=G_{12}\\ &\Delta=\frac{1-\nu_{32}\nu_{23}-\nu_{21}\nu_{12}-\nu_{13}\nu_{31}-2\nu_{32}\nu_{21}\nu_{13}}{E_1E_2E_3}\end{aligned} \tag{20}$$

Moreover by considering of the Pasternak foundation model, total energy of the plate is as:

$$U=\frac{1}{2}\int_V\left[\boldsymbol{\varepsilon}^T\boldsymbol{\sigma}+\boldsymbol{\gamma}^T\boldsymbol{\tau}\right]dV+\frac{1}{2}\int_A\left[k_w w^2+k_s\left[\left(\frac{\partial w}{\partial x}\right)^2+\left(\frac{\partial w}{\partial y}\right)^2\right]\right]dA+\int_A[fw]dA \tag{21}$$

where f is the applied load, k_w and k_s are coefficients of Winkler and Pasternak foundation. If the foundation is modeled as the linear Winkler foundation, the coefficient k_s in Eq. (21) is zero.

4 MESH-FREE NUMERICAL ANALYSIS

In this paper, the moving least square shape functions introduced by Lancaster and Salkauskas [38] is used for approximation of displacement vector in the weak form of motion equation. Displacement vector ***d*** can be approximated by MLS shape functions as follows:

$$\hat{\mathbf{d}}=\sum_{i=1}^{N}\phi_i d_i \tag{22}$$

where N is the total number of nodes, $\hat{\mathbf{d}}$ is virtual nodal values vector and ϕ_i is MLS shape function of node located at $\boldsymbol{X}(x,y)=\boldsymbol{X}_i$ and they are defined as follows:

$$\hat{\mathbf{d}}=\left[\hat{u}_i\ ,\hat{v}_i\ ,\hat{w}_i\ ,\hat{\theta}_{\hat{x}}\ ,\hat{\theta}_{\hat{y}}\right]^T \tag{23}$$

and

$$\phi_i(\mathbf{X}) = \underbrace{\mathbf{P^T}(\mathbf{X})\left[\mathbf{H}(\mathbf{X})\right]^{-1} W(\mathbf{X}-\mathbf{X}_i)\mathbf{P}(\mathbf{X}_i)}_{(1\times 1)} \tag{24}$$

In the above equation, W is cubic Spline weight function, $\boldsymbol{P}$ is base vector and $\boldsymbol{H}$ is moment matrix and are defined as follows:

$$\mathbf{P}(\mathbf{X}) = [1, x, y]^T \tag{25}$$

$$\mathbf{H}(\mathbf{X}) = \left[\sum_{i=1}^{n} W(\mathbf{X}-\mathbf{X}_i)\mathbf{P}(\mathbf{X}_i)\mathbf{P}^{\mathbf{T}}(\mathbf{X}_i)\right] \tag{26}$$

By using of the MLS shape function, Eq. (17) can be written as:

$$\boldsymbol{\varepsilon} = \mathbf{B}_m\hat{\mathbf{d}} + z\mathbf{B}_b\hat{\mathbf{d}} \quad , \quad \boldsymbol{\gamma} = \mathbf{B}_s\hat{\mathbf{d}} \tag{27}$$

In which

$$\mathbf{B}_m = \begin{bmatrix} \phi_{i,x} & 0 & 0 & 0 & 0 \\ 0 & \phi_{i,y} & 0 & 0 & 0 \\ \phi_{i,y} & \phi_{i,x} & 0 & 0 & 0 \end{bmatrix}, \mathbf{B}_b = \begin{bmatrix} 0 & 0 & 0 & \phi_{i,x} & 0 \\ 0 & 0 & 0 & 0 & \phi_{i,y} \\ 0 & 0 & 0 & \phi_{i,y} & \phi_{i,x} \end{bmatrix}, \mathbf{B}_s = \begin{bmatrix} 0 & 0 & \phi_{i,y} & 0 & \phi_i \\ 0 & 0 & \phi_{i,x} & \phi_i & 0 \end{bmatrix} \tag{28}$$

Also for elastic foundation, $\boldsymbol{\varphi}_w$ and $\mathbf{B}_P$ can be defined as following:

$$\boldsymbol{\varphi}_w = \begin{bmatrix} 0 & 0 & \varphi_i & 0 & 0 \end{bmatrix}, \mathbf{B}_p = \begin{bmatrix} 0 & 0 & \varphi_{i,x} & 0 & 0 \\ 0 & 0 & \varphi_{i,y} & 0 & 0 \end{bmatrix} \tag{29}$$

Substitution of Eqs. (19) and (27) in Eq. (21) leads to:

$$\begin{aligned} U = {} & \frac{1}{2}\int_A \hat{\mathbf{d}}\int_z \left[\mathbf{B}_m^T\mathbf{A}\mathbf{B}_m + \mathbf{B}_m^T\bar{\mathbf{B}}\mathbf{B}_b + \mathbf{B}_b^T\bar{\mathbf{B}}\mathbf{B}_m + \mathbf{B}_b^T\mathbf{D}\mathbf{B}_b + \mathbf{B}_s^T\mathbf{A}_s\mathbf{B}_s\right] dz\hat{\mathbf{d}}dA \\ & \frac{1}{2}\int_A \left[\boldsymbol{\varphi}_w^T k_w \boldsymbol{\varphi}_w + \mathbf{B}_p^T k_s \mathbf{B}_p\right]\hat{\mathbf{d}}dA + \frac{1}{2}\int_A \boldsymbol{\varphi}_w^T f\, dA \end{aligned} \tag{30}$$

In which the components of the extensional stiffness $\mathbf{A}$, bending-extensional coupling stiffness $\bar{\mathbf{B}}$, bending stiffness $\mathbf{D}$ and transverse shear stiffness are defined as:

$$(\mathbf{A}, \bar{\mathbf{B}}, \mathbf{D}) = \int_{-h/2}^{h/2} \mathbf{Q}_b(1, z, z^2)dz \quad , \quad \mathbf{A}_s = \alpha\int_{-h/2}^{h/2} \mathbf{Q}_s dz \tag{31}$$

It can be noticed that the arrays of bending-extensional coupling stiffness matrix, $\bar{\mathbf{B}}$, are zero for symmetric laminated composites. Finally, by a derivative with respect to displacement vector, $\hat{\mathbf{d}}$, the Eq. (30) can be expressed as:

$$\mathbf{K}\hat{\mathbf{d}} = \mathbf{F} \tag{32}$$

In which, $\mathbf{K}$ and $\mathbf{F}$ are stiffness matrix and force vector, respectively and are defined as:

$$\mathbf{K} = \mathbf{K}_m + \mathbf{K}_b + \mathbf{K}_s + \mathbf{K}_w + \mathbf{K}_p \tag{33}$$

$$\mathbf{F} = \int_A \boldsymbol{\varphi}_w^T f dA \tag{34}$$

In which, $\mathbf{K}_m$, $\mathbf{K}_b$ and $\mathbf{K}_s$ are stiffness matrixes of extensional, bending-extensional and bending, respectively and also, $\mathbf{K}_w$ and $\mathbf{K}_p$ are stiffness matrixes that represented the Winkler and Pasternak elastic foundations. They are defined as:

$$\mathbf{K}_m = \int_A \left[\mathbf{B}_m^T \mathbf{A} \mathbf{B}_m + \mathbf{B}_m^T \overline{\mathbf{B}} \mathbf{B}_b + \mathbf{B}_b^T \overline{\mathbf{B}} \mathbf{B}_m\right] dA \,,\ \mathbf{K}_b = \int_A \mathbf{B}_b^T \mathbf{D} \mathbf{B}_b dA \ ,\ \mathbf{K}_s = \int_z \mathbf{B}_s^T \mathbf{A}_s \mathbf{B}_s dA \tag{35}$$

$$\mathbf{K}_w = \int_A \boldsymbol{\varphi}_w^T k_w \boldsymbol{\varphi}_w dA \ \ ,\ \mathbf{K}_p = \int_A \mathbf{B}_p^T k_s \mathbf{B}_p dA \tag{36}$$

For numerical integration, problem domain is discretized to a set of background cells with gauss points inside each cell. Then global stiffness matrix $\mathbf{K}$ is obtained numerically by sweeping all gauss points.

Imposition of essential boundary conditions in the system of Eq. (32) is not possible. Because MLS shape functions don't satisfy the Kronecker delta property. In this work transformation method is used for imposition of essential boundary conditions. For this purpose transformation matrix is formed by establishing relation between nodal displacement vector $\mathbf{d}$ and virtual displacement vector $\hat{\mathbf{d}}$.

$$\mathbf{d} = \mathbf{T}\hat{\mathbf{d}} \tag{37}$$

T is the transformation matrix that is a (5*N*×5*N*) matrix and for each node is defined as:

$$\mathbf{T} = \begin{bmatrix} \phi_1(x_1)\times\mathbf{I}_{(5\times5)} & \phi_1(x_2)\times\mathbf{I}_{(5\times5)} & . & . & \phi_1(x_N)\times\mathbf{I}_{(5\times5)} \\ \phi_2(x_1)\times\mathbf{I}_{(5\times5)} & \phi_2(x_2)\times\mathbf{I}_{(5\times5)} & . & . & \phi_2(x_N)\times\mathbf{I}_{(5\times5)} \\ . & . & . & . & . \\ . & . & . & . & . \\ \phi_N(x_1)\times\mathbf{I}_{(5\times5)} & \phi_N(x_2)\times\mathbf{I}_{(5\times5)} & . & . & \phi_N(x_N)\times\mathbf{I}_{(5\times5)} \end{bmatrix} \tag{38}$$

where $\mathbf{I}_{(5\times5)}$ is an identity matrix of size 5. By using Eq. (37), system of linear Eq. (32) can be rearranged to:

$$\hat{\mathbf{K}}\mathbf{d} = \hat{\mathbf{F}} \tag{39}$$

where,

$$\hat{\mathbf{K}} = \mathbf{T}^{-T}\mathbf{K}\mathbf{T}^{-1} \ \ ,\ \hat{\mathbf{F}} = \mathbf{T}^{-T}\mathbf{F} \tag{40}$$

Now the essential boundary conditions can be enforced to the modified equations system (39) easily like the finite element method.

5 RESULTS AND DISCUSSIONS

In the following simulations, bending behavior of sandwich plates with nanocomposite face sheets is characterized which are functionally graded reinforced by aggregated CNT. For the nanocomposites, PMMA or Poly (methyl-methacrylate) is selected as the matrix material. The relevant material properties for CNTs and PMMA are as follows [39]:

$E_1^{CN} = 5.6466\ TPa$, $E_2^{CN} = 7.0800\ TPa$, $G_{12}^{CN} = 1.9445\ TPa$, $\rho^{CN} = 1400\ Kg/m^3$, $\upsilon_{12}^{CN} = 0.175$ for (10,10) SWCNTs

$E^m = 2.5GPa$, $\rho^m = 1150\,Kg/m^3$, $\upsilon^m = 0.34$ for PMMA

In this work, bending behavior and mechanical characteristics of sandwich plates with FG-CNTRC face sheets were investigated using several numerical examples. The sandwich plates were assumed resting on Winkler-Pasternak elastic foundation and the developed mesh-free method is used. At first, validation of the developed mesh-free method on bending behavior of plates is examined. Then, based on the examined mesh-free method, new results about bending characteristics of the sandwich plates on the elastic foundation will be reported. In the following examples, the foundation parameters are presented in the non-dimensional form of $K_w=k_wa^4/D$ and $K_s=k_sa^2/D$, in which $D=E_mh^3/12(1-\upsilon_m^2)$ is a reference bending rigidity of the plate. Also, the non-dimensional deflection of the sandwich plates is defined as [40]:

$$\hat{q} = 10^2 E_m h^3 q / f_0 a^4 \tag{41}$$

In which, f_0 is the value of applied (concentrated or uniformly distributed) load and q is central deflection.

5.1 Validation of models

Convergence and accuracy are two main parameters for evaluation of each numerical method. So, consider a simply supported homogeneous square plate under uniformly distributed load, f_0. Fig. 4 illustrates an excellent convergence and accuracy for the developed mesh-free method in central non-dimensional deflection $\hat{q}$, of the plate with h/a=0.02 in comparing with exact results which are reported by Akhras et al. [41]. Also, Table 1. discloses a good agreement between central non-dimensional deflection which are derived by the mesh-free method and FEM results which are reported by Zhu et al. [42] for square clamped UD-CNTRC plates with the values of b/h (=50, 20 and 10).

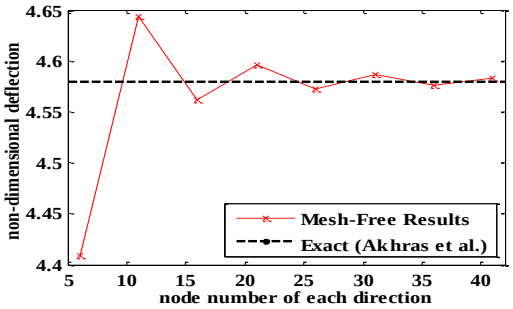

Fig.4
Convergence of the central non-dimensional deflection, $\hat{q}$, for different number of node in each direction.

Table 1
Comparison of the central non-dimensional deflections, $\hat{q}$, in clamped square plates reinforced by straight CNTs.

b/h	Mesh-Free (35×35)	Zhu et al. [42]
50	0.1690	0.1698
20	8.309×10^{-2}	8.561×10^{-2}
10	1.353×10^{-3}	1.412×10^{-3}

5.2 Bending behavior of FG-CNTRC sandwich plates

To investigate bending behavior, consider square sandwich plates with aggregated CNT-reinforced face sheets subjected to uniformed distribution load of f_0=-1e4 on top face, resting on Winkler-Pasternak foundation and with two clamped (C) and two simply supported (S) edges(CSCS). Fig. 5 illustrates the effect of aggregation degrees (μ,η) on the non-dimensional central deflection $\hat{q}$, for the square sandwich plates with constant CNT volume fraction (UD) of f_r=0.2, h/a = 0.15, h_f/h = 0.15, K_w=50 and K_s=5. It can be seen that increasing of cluster volumes (μ) or decreasing of CNT concentration in clusters (decreasing η from unit), due to making a better CNT distribution in the matrix, decrease the value of central deflection. Also, the aggregation degree of (μ=η) shows the fully-dispersed state of CNTs in the matrix and indicates the best reinforcement behavior in bending analysis.

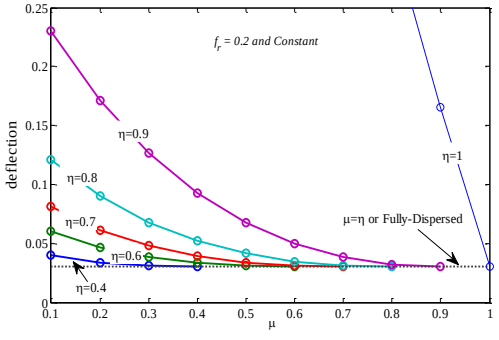

Fig.5
Central non-dimensional deflections, $\hat{q}$, for square CSCS sandwich plates with f_r=0.2, h/a = 0.15, h_f/h = 0.15, K_w=50 and K_s=5.

Table 2. lists the non-dimensional central deflection of the sandwich plates for the various values of maximum volume fractions of CNTs and clusters when η=1, h/a = 0.15, h_f/h = 0.15, K_w=50 and K_s=5. It can be seen that increasing of μ, increasing of $f_{r_{\max}}$ or decreasing of the CNT volume fraction exponent lead to decrease in central deflection of the sandwich plates with FG-CNTRC face sheets. The sharp effect of increasing in cluster volume versus other factors is very obvious. So, it can be concluded that the effect of CNT distribution is much more important than the effect of increasing CNT volume.

Table 2
Central non-dimensional deflections, $\hat{q}$, for square CSCS sandwich plates with η = 1, h/a = 0.15, h_f/h = 0.15, K_w=50 and K_s=5.

μ	$f_{r_{\max}}$	n=0.1	n=1	n=10
0.3	0.1	1.5711	1.5933	1.8927
	0.2	1.5663	1.5794	1.8614
	0.3	1.5649	1.5743	1.8447
0.5	0.1	1.1777	1.2281	1.7064
	0.2	1.1630	1.1945	1.6443
	0.3	1.1584	1.1817	1.6117
0.8	0.1	0.5666	0.6613	1.3163
	0.2	0.5256	0.5872	1.1771
	0.3	0.5116	0.5587	1.1084
1	0.1	0.1319	0.2197	0.7675
	0.2	0.0628	0.1096	0.4569
	0.3	0.0385	0.0696	0.3159

Returning now to the effects of sandwich plate dimension, Table 3 investigates the effects of plate thickness, face sheet thicknesses and aspect ratio of the CSCS sandwich plates with μ = 0.3, η = 1, $f_{r_{\max}}$ =0.2, K_w=50 and K_s=5. It can be seen that increasing of the face sheet thicknesses may decrease the deflection. Actually, the deflection of the sandwich plate is decreased by increasing of plate's thickness, but due to the definition of $\hat{q}$ in Eq. (41), Table 3. shows that the deflection is increased by increasing of h. Finally, the deflection was dramatically increased by increasing the ratio of b/a from 1 to 3 because the sandwich plate nearly shows the sandwich beam's manners.

Table 3
Central non-dimensional deflections, $\hat{q}$, for CSCS sandwich plates with μ = 0.3, η = 1, $f_{r_{\max}}$ =0.2, K_w=50 and K_s=5.

h/a	h_f/h	b/a = 1			b/a = 3		
		n=0.1	n=1	n=10	n=0.1	n=1	n=10
0.1	0.1	1.4530	1.4644	1.6904	5.4672	5.4990	6.0982
	0.15	1.3395	1.3514	1.6110	5.1535	5.1879	5.8952
	0.2	1.2618	1.2732	1.5441	4.9372	4.9704	5.7200
0.15	0.1	1.6930	1.7052	1.9461	5.6414	5.6729	6.2655
	0.15	1.5663	1.5794	1.8614	5.3273	5.3616	6.0647
	0.2	1.4763	1.4892	1.7890	5.1082	5.1417	5.8910
0.2	0.1	1.9859	1.9990	2.2555	5.8394	5.8704	6.4513
	0.15	1.8444	1.8589	2.1652	5.5260	5.5601	6.2544
	0.2	1.7403	1.7549	2.0870	5.3039	5.3375	6.0833

The effects of sandwich plate boundary conditions and elastic foundation coefficients are examined in Table 4. and Table 5. for the square sandwich plates with $\mu = 0.3$, $\eta = 1$, $f_{r_{max}} = 0.2$, $h/a = 0.15$ and $h_f/h = 0.15$ in two cases of without and resting on elastic foundation. It can be seen that fully clamped sandwich plates and the sandwich plates with only two simply supported edges have the minimum and maximum values of central deflection, respectively (F: free edge). So, decreasing of the boundary condition constrains increases the values of plate deflection. Also, the elastic foundation could decrease the sandwich plate deflection noticeably and the effect of shear coefficient are more than normal (Winkler) one.

Table 4

Central non-dimensional deflections, $\hat{q}$, for square sandwich plates with $\mu = 0.3$, $\eta = 1$, $f_{r_{max}} = 0.2$, $h/a = 0.15$ and $h_f/h = 0.15$.

B.C.	$K_w = 0$, $K_s = 0$			$K_w = 50$, $K_s = 5$		
	n=0.1	n=1	n=10	n=0.1	n=1	n=10
CCCC	1.3017	1.3144	1.8572	1.1528	1.1628	1.5675
CSCS	1.8426	1.8609	2.6493	1.5663	1.5794	2.1125
CFCF	2.4106	2.4345	3.4629	2.0257	2.0425	2.7181
SSSS	3.1651	3.1980	4.6680	2.4492	2.4688	3.2620
SFSF	9.5691	9.6705	14.2833	5.5065	5.5399	6.7968

Table 5

Central non-dimensional deflections, $\hat{q}$, for square CSCS sandwich plates with $\mu = 0.3$, $\eta = 1$, $f_{r_{max}} = 0.2$, $h/a = 0.15$ and $h_f/h = 0.15$.

K_w	K_s	n=0.01	n=0.1	n=1	n=10	n=100
20	2	1.7210	1.7214	1.7373	2.0849	2.4055
	5	1.6141	1.6144	1.6284	1.9298	2.2010
	10	1.4625	1.4628	1.4743	1.7168	1.9276
50	2	1.6666	1.6670	1.6819	2.0056	2.3007
	5	1.5659	1.5663	1.5794	1.8614	2.1125
	10	1.4227	1.4229	1.4338	1.6621	1.8589
100	2	1.5829	1.5832	1.5967	1.8856	2.1442
	5	1.4915	1.4919	1.5038	1.7571	1.9792
	10	1.3607	1.3609	1.3708	1.5779	1.7542

Finally, in the last case, both CNT and cluster volume fractions are assumed to be functionally graded along the face sheet thickness. Fig. 6 shows the non-dimensional central deflection versus CNT volume fraction exponent (in logarithm-scale) for three constant values of μ (= 0.1, 0.15, 0.3) and a linear variation of μ from zero at inner face to 0.3 at outer face of each face sheets when $\eta = 1$, $f_{r_{max}} = 0.2$, $h/a = 0.15$, $h_f/h = 0.15$, K_w=50 and K_s=5. It is clear that increasing of the CNT volume fraction exponent increases the deflection of sandwich plates in all cases. Also, comparison between the results of $\mu = 0.15$ and graded μ disclose that functionally graded distribution of clusters leads to less deflection when the value of cluster volume are the same.

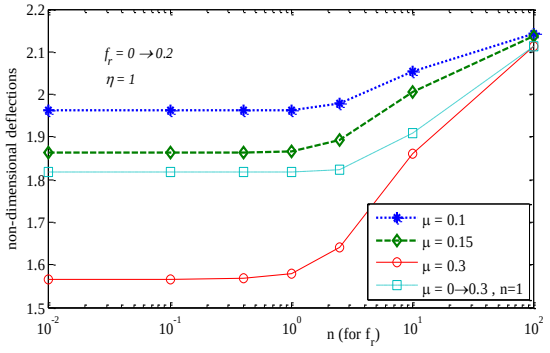

Fig.6
Central non-dimensional deflections, $\hat{q}$, for square CSCS sandwich plates with $\eta = 1$, $f_{r_{max}} = 0.2$, $h/a = 0.15$, $h_f/h = 0.15$, K_w=50 and K_s=5.

6 CONCLUSIONS

In this paper, an FSDT based mesh-free method and Eshelby-Mori-Tanaka approach were used to analyze the bending behavior of sandwich plates with aggregated CNT-reinforced composite face sheets by considering of the effects of CNT aggregation. In the face sheets, volume fraction of CNTs and their clusters were considered to be changed along the thickness. The sandwich plates were assumed resting on Winkler-Pasternak elastic foundation and the effects of CNTs volume fraction and their distribution, the degree of CNT aggregation, boundary conditions and geometric dimensions were investigated on the bending behavior of the sandwich plates. The following results were obtained from this analysis:

- The developed mesh-free method has an excellent convergence and accuracy on the bending behavior of sandwich plates.
- Increasing of cluster volumes (μ) or decreasing in CNT concentration of cluster (decreasing η from unit) decrease the value of central deflection.
- Increasing of CNT volume or decreasing of the CNT volume fraction exponent lead to decrease in central deflection of the sandwich plates.
- The deflections of rectangular sandwich plates are more than the deflection of square sandwich plates.
- Elastic foundation could decrease the sandwich plate deflections noticeably.
- In the same value of cluster volume, functionally graded distribution of clusters leads to less deflection in the sandwich plates.

REFERENCES

[1] Iijima S., Ichihashi T., 1993, Single-shell carbon nanotubes of 1-*nm* diameter, *Nature* **363**: 603-605.

[2] Thai H., Choi D., 2011, A refined plate theory for functionally graded plates resting on elastic foundation, *Composites Science and Technology* **71**(16): 1850-1858.

[3] Shen H., 2009, Nonlinear bending of functionally graded carbon nanotube-reinforced composite plates in thermal environments, *Composite Structures* **91**(1): 9-19.

[4] Alibeigloo A., 2013, Static analysis of functionally graded carbon nanotube-reinforced composite plate embedded in piezoelectric layers by using theory of elasticity, *Composite Structures* **95**: 612-622.

[5] Shariyat M., Darabi E., 2013, A variational iteration solution for elastic – plastic impact of polymer / clay nanocomposite plates with or without global lateral deflection , employing an enhanced contact law, *International Journal of Mechanical Sciences* **67**: 14-27.

[6] Pourasghar A., Kamarian S., 2013,Three-dimensional solution for the vibration analysis of functionally graded multiwalled carbon nanotubes/phenolic nanocomposite cylindrical panels on elastic foundation, *Polymer Composites* **34**(12): 2040-2048.

[7] Malekzadeh P., Zarei A. R., 2014, Free vibration of quadrilateral laminated plates with carbon nanotube reinforced composite layers, *Thin Walled Structures* **82**: 221-232.

[8] Kundalwal S. I., Meguid S. A., 2015, Effect of carbon nanotube waviness on active damping of laminated hybrid composite shells, *Acta Mechanica* **226**: 2035-2052.

[9] Mohammadimehr M., Navi B. R., Ghorbanpour Arani A., 2016, Modified strain gradient Reddy rectangular plate model for biaxial buckling and bending analysis of double-coupled piezoelectric polymeric nanocomposite reinforced by FG-SWNT, *Composites Part B* **87**: 132-148.

[10] Ghorbanpour Arani A., Mosayyebi M., Kolahdouzan F., Kolahchi R., Jamali M., 2017, Refined zigzag theory for vibration analysis of viscoelastic functionally graded carbon nanotube reinforced composite microplates integrated with piezoelectric layers, *Proceedings of the Institution of Mechanical Engineers Part G, Journal of Aerospace Engineering* **231**(13): 2464-2478.

[11] Ghorbanpour Arani A., Jafari G. S., 2015, Nonlinear vibration analysis of laminated composite Mindlin micro/nano-plates resting on orthotropic Pasternak medium using DQM, Applied *Mathematics and Mechanics* **36**(8): 1033-1044.

[12] Ghorbanpour Arani A., Haghparast E., Ghorbanpour Arani A. H., 2016, Size-dependent vibration of double-bonded carbon nanotube-reinforced composite microtubes conveying fluid under longitudinal magnetic field, *Polymer Composites* **37**(5): 1375-1383.

[13] Pourasghar A., Yas M., Kamarian S., 2013, Local aggregation effect of CNT on the vibrational behavior of four-parameter continuous grading nanotube-reinforced cylindrical panels, *Polymer Composites* **34**: 707-721.

[14] Aragh B. S., Hedayati H., 2012, Eshelby-Mori-Tanaka approach for vibrational behavior of continuously graded carbon nanotube-reinforced cylindrical panels, *Composites Part B* **43**(4): 1943-1954.

[15] Tahouneh V., Yas M. H., 2014, Influence of equivalent continuum model based on the Eshelby-Mori-Tanaka scheme on the vibrational response of elastically supported thick continuously graded carbon nanotube-reinforced annular

plates, *Polymer Composites* **35**: 1644-1661.
[16] Moradi-Dastjerdi R., Payganeh G., Malek-Mohammadi H., 2015, Free vibration analyses of functionally graded CNT reinforced nanocomposite sandwich plates resting on elastic foundation, *Journal of Solid Mechanics* **7**(2): 158-172.
[17] Moradi-Dastjerdi R., Malek-Mohammadi H., 2017, Biaxial buckling analysis of functionally graded nanocomposite sandwich plates reinforced by aggregated carbon nanotube using improved high-order theory, *Journal of Sandwich Structures & Materials* **19**(6): 736-769.
[18] Moradi-Dastjerdi R., Malek-Mohammadi H., Momeni-Khabisi H., 2017, Free vibration analysis of nanocomposite sandwich plates reinforced with CNT aggregates, *ZAMM - Journal of Applied Mathematics and Mechanics / Zeitschrift für Angewandte Mathematikund Mechanik* **97**(11): 1418-1435.
[19] Moradi-Dastjerdi R., Malek-Mohammadi H., 2017, Free vibration and buckling analyses of functionally graded nanocomposite plates reinforced by carbon nanotube, *Mechanics of Advanced Materials and Structures* **4**(1): 59-73.
[20] Lei Z. X., Liew K. M., Yu J. L., 2013, Buckling analysis of functionally graded carbon nanotube-reinforced composite plates using the element-free kp -Ritz method, *Composite Structures* **98**: 160-168.
[21] Moradi-Dastjerdi R., Sheikhi M. M., Shamsolhoseinian H. R., 2014, Stress distribution in functionally graded nanocomposite cylinders reinforced by wavy carbon nanotube, *International Journal of Advanced Manufacturing Technology* **7**(4): 43-54.
[22] Sheikhi M. M., Shamsolhoseinian H. R., Moradi-Dastjerdi R., 2016, Investigation on stress distribution in functionally graded nanocomposite cylinders reinforced by carbon nanotubes in thermal environment, *International Journal of Advanced Manufacturing Technology* **9**(2): 81-93.
[23] Moradi-Dastjerdi R., Pourasghar A., 2016, Dynamic analysis of functionally graded nanocomposite cylinders reinforced by wavy carbon nanotube under an impact load, *Journal of Vibration and Control* **22**: 1062-1075.
[24] Moradi-Dastjerdi R., Payganeh G., 2017, Transient heat transfer analysis of functionally graded CNT reinforced cylinders with various boundary conditions, *Steel and Composite Structures* **24**(3): 359-367.
[25] Shams S., Soltani B., 2015, The effects of carbon nanotube waviness and aspect ratio on the buckling behavior of functionally graded nanocomposite plates using a meshfree method, *Polymer Composites* **38**: 1-11.
[26] Moradi-Dastjerdi R., 2016, Wave propagation in functionally graded composite cylinders reinforced by aggregated carbon nanotube, *Structural Engineering and Mechanics* **57**(3): 441-456.
[27] Moradi-Dastjerdi R., Payganeh G., Tajdari M., 2017, The effects of carbon nanotube orientation and aggregation on static behavior of functionally graded nanocomposite cylinders, *Journal of Solid Mechanics* **9**(1): 198-212.
[28] Zhang L. W., Lei Z. X., Liew K. M., 2015, An element-free IMLS-Ritz framework for buckling analysis of FG – CNT reinforced composite thick plates resting on Winkler foundations, *Engineering Analysis with Boundary Elements* **58**: 7-17.
[29] Zhang L. W., Song Z. G., Liew K. M., 2015, Nonlinear bending analysis of FG-CNT reinforced composite thick plates resting on Pasternak foundations using the element-free IMLS-Ritz method, *Composite Structures* **128**: 165-175.
[30] Moradi-Dastjerdi R., Payganeh G., Rajabizadeh Mirakabad S., . Jafari Mofrad Taheri M., 2016, Static and free vibration analyses of functionally graded nano- composite plates reinforced by wavy carbon nanotubes resting on a pasternak elastic foundation, *Mechanics of Advanced Materials and Structures* **3**: 123-135.
[31] Moradi-Dastjerdi R., Momeni-Khabisi H., 2016, Dynamic analysis of functionally graded nanocomposite plates reinforced by wavy carbon nanotube, *Steel and Composite Structures* **22**(2): 277-299.
[32] Shi D., Feng X., Huang Y. Y., Hwang K. C., Gao H., 2004, The effect of nanotube waviness and agglomeration on the elastic property of carbon nanotube- reinforced composites, *Journal of Engineering Materials and Technology* **126**: 250-257.
[33] Eshelby J. D., 1957, The determination of the elastic field of an ellipsoidal inclusion, and related problems, *Proceedings of the Royal Society of London Series A* **241**: 376-396.
[34] Mura T., 1982, *Micromechanics of Defects in Solids,* The Hague Martinus Nijhoff Pub.
[35] Prylutskyy Y., Durov S., Ogloblya O., Buzaneva E., Scharff P., 2000, Molecular dynamics simulation of mechanical, vibrational and electronic properties of carbon nanotubes, *Computational Materials Science* **17**: 352-355.
[36] Reddy J. N., *2004, Mechanics of Laminated Composite Plates and Shells: Theory and Analysis*, CRC Press.
[37] Efraim E., Eisenberger M. Ã., 2007, Exact vibration analysis of variable thickness thick annular isotropic and FGM plates, *Journal of Sound and Vibration* **299**: 720-738.
[38] Lancaster P., Salkauskas K., 1981, Surface generated by moving least squares methods, *Mathematics of Computation* **37**: 141-158.
[39] Shen H., 2011, Postbuckling of nanotube-reinforced composite cylindrical shells in thermal environments , Part I : Axially-loaded shells, *Composite Structures* **93**(8): 2096-2108.
[40] Ferreira A. J. M., Castro L. M. S., Bertoluzza S., 2009, A high order collocation method for the static and vibration analysis of composite plates using a first-order theory, *Composite Structures* **89**(3): 424-432.
[41] Akhras G., Cheung M., Li W., 1994, Finite strip analysis for anisotropic laminated composite plates using higher-order deformation theory, *Composite Structures* **52**: 471-477.
[42] Zhu P., Lei Z. X., Liew K. M., 2012, Static and free vibration analyses of carbon nanotube-reinforced composite plates using finite element method with first order shear deformation plate theory, *Composite Structures* **94**(4): 1450-1460.